Lentz, B. R., Barenholz, Y., & Thompson, T. E. (1975) *Chem. Phys. Lipids 15*, 216–221.
Lund-Katz, S., & Phillips, M. C. (1984) *Biochemistry 23*, 1130–1138.
Lund-Katz, S., & Phillips, M. C. (1986) *Biochemistry 25*, 1562–1568.
Markwell, M. A. K., Haas, S. M., Bieber, L. L., & Tolbert, N. E. (1978) *Anal. Biochem. 87*, 206–210.
McKay, H. A. C. (1938) *Nature (London) 142*, 997.
McLean, L. R., & Phillips, M. C. (1981) *Biochemistry 20*, 2893–2900.
McLean, L. R., & Phillips, M. C. (1982) *Biochemistry 21*, 4053–4059.
McLean, L. R., & Phillips, M. C. (1984) *Biochim. Biophys. Acta 776*, 21–26.
Phillips, M. C. (1972) *Prog. Surf. Membr. Sci. 5*, 139–221.
Phillips, M. C., & Chapman, D. (1968) *Biochim. Biophys. Acta 163*, 301–313.
Phillips, M. C., Johnson, W. J., & Rothblat, G. H. (1987) *Biochim. Biophys. Acta 906*, 223–276.
Salem, L. (1962) *Can. J. Biochem. Physiol. 40*, 1287–1298.
Schmidt, C. F., Barenholz, Y., & Thompson, T. E. (1977) *Biochemistry 16*, 2649–2656.
Shinitzky, M., & Barenholz, Y. (1974) *J. Biol. Chem. 249*, 2652–2657.
Shipley, G. G., Avecilla, L. S., & Small, D. M. (1974) *J. Lipid Res. 15*, 124–131.
Silvius, J. R. (1982) in *Lipid–Protein Interactions* (Jost, P. C., & Griffith, O. H., Eds.) Vol. 2, pp 239–281, Wiley-Interscience, New York.
Sokoloff, L., & Rothblat, G. H. (1974) *Proc. Soc. Exp. Biol. Med. 146*, 1166–1172.
Van Blitterswijk, W. J., Van deer Meer, B. W., & Hilkmann, H. (1987) *Biochemistry 26*, 1746–1756.
Van den Besselaar, A. M. H. P., Helmcamp, G. M., Jr., & Wirtz, K. W. A. (1975) *Biochemistry 14*, 1852–1858.
Weinstein, S., Wallace, B. A., Morrow, J. S., & Veatch, W. R. (1980) *J. Mol. Biol. 143*, 1–19.
Yeagle, P. L., & Young, J. E. (1986) *J. Biol. Chem. 261*, 8175–8181.
Yedgar, S., Cohen, R., Gatt, S., & Barenholz, Y. (1982) *Biochem. J. 201*, 597–603.

Structure of a Bent DNA: Two-Dimensional NMR Studies on $d(GAAAATTTTC)_2$†

Mukti H. Sarma, Goutam Gupta, and Ramaswamy H. Sarma*
Institute of Biomolecular Stereodynamics, State University of New York at Albany, Albany, New York 12222
Received January 4, 1988; Revised Manuscript Received March 2, 1988

ABSTRACT: Intrinsic DNA bending is caused by specific DNA sequences. The decamer $d(GA_4T_4C)_2$, when it repeats in a synthetic polymer or in kinetoplast DNA, results in a macroscopic bending of the molecule as a whole. We employed high-resolution two-dimensional NMR methods to examine the intrinsic structural properties of the $d(GA_4T_4C)_2$ duplex in solution. Examination of the NOESY data at 50- and 100-ms mixing times indicated that the kinds of observed NOEs can originate if each of the ten nucleotidyl residues belongs to the B-DNA family, i.e., C2′-endo,anti. However, the *degree* of observed NOE intensities from the A-T junction as well as the observed AH2–AH2 cross-peaks from adjacent AT pairs could not be rationalized on the basis of a straight B-DNA model but could be explained by only a B-DNA model with some structural discontinuity at the A-T junction—the site of 2-fold symmetry in the molecule. In view of the fact that the degree of observed NOE intensities can be complicated by spin diffusion and by fine structural distortion, we have resorted to the use of quantitative theoretical NOESY simulation (which takes into account primary, secondary, and higher orders of NOE) to delineate the structural discontinuity at the A-T junction and to arrive at a structure for the duplex $d(GA_4T_4C)_2$. We propose a "junction B-DNA model" which can quantitatively explain the 2D NOESY data at 100- and 50-ms mixing times. In this model the two structural blocks in the molecule, i.e., $d(GA_4)$·$d(T_4C)$ and $d(T_4C)$·$d(GA_4)$, are conformationally equivalent and are connected at the A-T junction where the base pairs are stably stacked, but the two local structural frames do not coincide in space. This model can create an overall bending of 10° with a center of curvature 50 Å away from the center of the duplex. It is the thesis of this paper that the observed bending in polymers with a repeat of $d(GA_4T_4C)_2$ and the bending in natural DNAs where A_nT_n·A_nT_n repeats are present originate at the oligonucleotide repeat level.

DNA bending refers to the phenomenon in which the long axis of a DNA duplex is curved. Bending of DNA can be classified in two broad categories: (i) intrinsic bending due to specific base sequences, e.g., bending of kinetoplast DNA (Hagerman, 1984; Kifchin et al., 1986; Marini et al., 1982), and (ii) induced bending, e.g., DNA bending in a protein–DNA complex (Frederick et al., 1984). However, fine structural details of a bent DNA in solution have not been determined so far experimentally. We believed that the decamer $d(GA_4T_4C)_2$, a prototype of a bending center in the kinetoplast DNA, would be an ideal model system to work

† This research is supported by a grant from the National Institutes of Health (GM29787) and by a contract from the National Foundation for Cancer Research. The high-field NMR experiments were performed at the NMR facility for Biomolecular Research located at the F. Bitter National Magnet Laboratory, MIT. The NMR facility is supported by Grant RR00995 from Division of Research Resources of the NIH and by the National Science Foundation under Contract C-670.

0006-2960/88/0427-3423$01.50/0

with. Hagerman (1986) showed that the polymer with a repeat of $d(GA_4T_4C)_2$ behaves like a bent molecule, i.e., retarded on an electrophoretic gel. Therefore, our primary interest was to examine whether $d(GA_4T_4C)_2$ possessed an intrinsic structural property upon which the macroscopic bending of the polymer with the same repeat could be explained. Theoretical studies have indicaed that DNA could be bent by the introduction of AA·TT wedges (Trifonov, 1986; Ulanovsky & Trifonov, 1987; Olson et al., 1988) and by the introduction of abrupt junctions between conformationally nonidentical structural blocks (Levene & Crothers, 1983). In view of the fact that both the models should involve very small departure from a normal straight DNA at the level of the decamer $d(GA_4T_4C)_2$, we focused our attention in detecting any subtle change in the conformation of $d(GA_4T_4C)_2$ in solution from that of a normal straight DNA by using quantitative 2D NMR spectroscopy.

Materials and Methods

DNA Synthesis and Purification. The decamer $d(GA_4T_4C)_2$ was synthesized on a DNA synthesizer (Applied Biosystems Model 380A) following the method of Matteinci et al. (1981). The product was purified on a 1.1 × 50 cm column of Sepharose Q (Pharmacia) with a linear gradient of 0.2–0.8 M NaCl in 10 mM NaOH (pH 12.0) and further purified by several ethanol precipitations.

NMR Spectroscopy. For both H_2O and D_2O samples, the DNA concentration was 2 mM in duplex and the salt concentration was 100 mM in NaCl [pH 7.0 in 10 mM sodium phosphate buffer with 1 mM ethylenediaminetetraacetic acid (EDTA)]. One-dimensional NMR spectra of $d(GA_4T_4C)_2$ in H_2O were recorded for temperatures of 5–30 °C, by use of a time-shared long pulse sequence. NOE difference spectra of $d(GA_4T_4C)_2$ at 12 °C in H_2O were recorded for presaturation times τ_m = 200 and 50 ms for the imino protons with a relaxation delay RD = 1.0 s and 5000 transients (NS).

The COSY spectrum of $d(GA_4T_4C)_2$ at 12 °C in D_2O was recorded with the pulse sequence $(RD–90°–t_1–90°–Acq)_{NS}$ in the pure absorption mode (States et al., 1982) with RD = 1.2 s and a data matrix (t_2 = 1024 × t_1 = 512) for NS = 64. NOESY spectra at τ_m = 100 and 50 ms were collected under the same conditions but with the pulse sequence $(RD–90°–t_1–90°–\tau_m–90°–Acq)_{NS}$.

NOESY Data Simulation. The NOESY intensities between protons i and j is computed from

$$C(i,j) \propto [\exp(-R\tau_m)]_{i,j} \ldots \quad (1)$$

where R is a cross-relaxation matrix ($N \times N$) spin system for a given τ_c [for details of the methodology and its application, see Keepers and James (1984) and Broido et al. (1985)]. The elements R_{ij} of the $N \times N$ relaxation matrix R can be computed from the knowledge of pairwise interproton distances in a model. For the purpose of our calculation we chose an isotropic correlation time for the molecule (as an approximation). The exponential term in eq 1 was computed as a series expansion until a numerical convergence was achieved. In our computational procedure primary and higher order NOEs are present as the first and higher order terms in the series expansion, i.e., eq 1. The problem of spin diffusion does not, therefore, create any complications because we do not compute pairwise interproton distances from the NOESY data. We compute the NOESY intensities for various peaks for a model with a given set of pairwise interproton distances by taking care of primary and higher orders of NOEs and refine the model until a satisfactory agreement is reached between the observed and calculated intensities.

Results

Assignment of the NH Protons. The temperature dependence of the imino protons (NH) of the G-C and A-T Watson–Crick pairs was monitored to study the duplex nature of the decamer $d(GA_4T_4C)_2$ in water at 100 mM NaCl (pH 7.0). It was observed that the decamer remained in the duplex state up to 30 °C. We chose 12 °C for performing the 1D NOE and 2D NOESY/COSY experiments because at this temperature both exchangeable NH (in H_2O) and nonexchangeable base protons H8/H6 H2/H5/CH3 (in D_2O) were best resolved. Figure 1A shows the downfield region of the 500-MHz ^1H NMR spectrum of $d(GA_4T_4C)_2$ duplex in H_2O at 12 °C. Notice four signals from N3H (of A-T) and one from N1H (of G-C)—as expected from the self-complementary decamer in the duplex state (see the inset of Figure 1). The N1H (G1) signal at 12.54 ppm from the terminal (G1-C10) pair was most sensitive to the temperature change. We performed 1D NOE experiments with five NH signals as irradiation sites at τ_m = 200 and 50 ms for determining the sequential assignment of the NH signals. With N1H of G1-C10 as a marker and by monitoring of the NOEs at τ_m = 200 and 50 ms, the following assignments were obtained from the spectra in Figure 1:

(*i*) *Spectrum B* (τ_m = *50 ms Showing the Primary NOE*). Notice two NOE sites from N1H (G1) of G1-C10 at 12.54 ppm—one at 13.81 ppm identified as N3H (T9) of A2-T9 and the other at 7.17 ppm assigned to H2(A2) of A2-T9.

(*ii*) *Spectrum C.* There were two NOE sites from N3H (T9) of A2-T9—in addition to the one at 7.17 ppm [H2(A2) of A2-T9], a signal was observed at 7.03 ppm belonging to H2(A3) of A3-T8 (see the inset of Figure 1). There was also an NOE in the NH region [i.e., to N3H(T8) of A3-T8], but it was partially hidden under the site of irradiation.

(*iii*) *Spectrum E.* Strong NOE from the signal at 13.76–7.03 ppm [H2(A3) of A3-T8] suggested the signal at 13.76 ppm belonged to N3H(T8) of A3-T8. Another strong signal at 7.07 ppm should then belong to H2(A4) of A4-T7. Irradiation of the signal at 13.76 ppm also results in partial irradiation of the N3H(T9) of A2-T9 at 13.81 ppm, and hence, we observe a smaller but noticeable NOE at H2(A2) of A2-T9 at 7.17 ppm.

(*iv*) *Spectrum D.* Strong NOE from the signal at 13.89 ppm to H2(A4) of A4-T7 at 7.07 ppm indicated that the signal at 13.89 should belong to N3H(T7) of A4-T7. The other signal at 7.34 ppm should belong to H2(A5) of A5-T6.

(*v*) *Spectrum F.* The remaining signal at 13.60 ppm belongs to N3H(T6) of A5-T6, irradiation of which results in a single site of NOE at H2(A5) of A5-T6 at 7.34 ppm.

Inspection of NOEs at τ_m = 200 and 50 ms revealed that the N3H(T) protons showed primary NOEs to H2(A) in the same base-pair and to H2(A) of the neighbor in the 3′ → 5′ direction—see the inset of Figure 1. Successive AT pairs are stacked in such a way that the distance *N3H of ith A·T pair–H2 of (i + 1)th A·T pair* is closer than the distance *N3H of ith A·T pair–H2 of (i–1)th A·T pair*. For example, in Figure 1F an NOE from T6·A5 is observed only at H2 of A5 and not at H2 of A4. This NOE pattern is consistent with a large propeller twist (≥15°) in the A·T pair.

Figure 2 shows the *H2(A) vs H2(A)* NOESY cross section for τ_m = 100 ms. One cross-peak is seen at (7.34, 7.07) ppm which according to our assignment should correspond to H2(A5)–H2(A4). Another cross-peak is expected for H2(A2)–H2(A3) at (7.17, 7.03) ppm; however, at the present NMR resolution this cross-peak is under the diagonal smear.

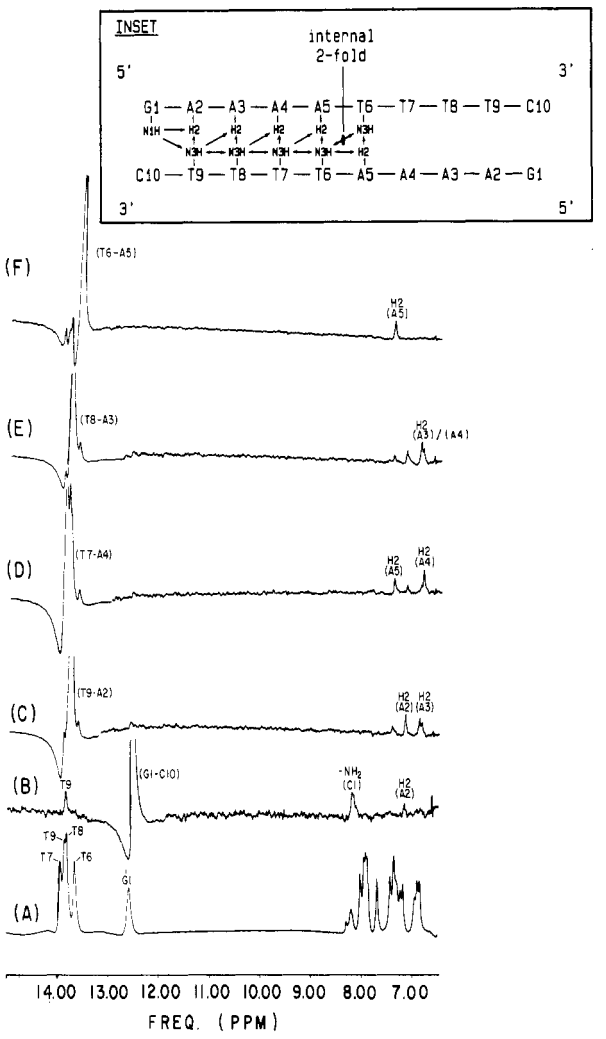

FIGURE 1: One-dimensional NOE spectra of the $d(GA_4T_4C)_2$ (see the inset) duplex in H_2O at 12 °C; the control spectrum (A) is also shown. The imino protons of chemically distinguishable base pairs were presaturated for τ_m = 50 ms. Comparison of similar NOE spectra for τ_m = 200 ms indicated that at τ_m = 50 ms we essentially observe the primary NOEs. In spectrum B, NH at 12.54 ppm of the G1-C10 pair is irradiated, and NOEs at (13.81, 7.17) ppm are identified as belonging to N3-H(T9) and H2(A2) of the A2-T9 pair. Spectrum C shows the NOE sites from the NH at 13.81 ppm of the A2-T9 pair; two strong sites of NOE in the H2 region belong to H2(A2) at 7.17 ppm and H2(A3) at 7.03 ppm. In spectrum E the signal at 13.76 ppm is irradiated (which also results in partial irradiation of the signal at 13.81 ppm); two strong NOEs are observed: one at 7.03 ppm, i.e., H2(A3), and the other at 7.07 ppm, i.e., H2(A4). Spectrum D shows two strong NOEs at 7.07 ppm, i.e., H2(A4), and 7.34 ppm, i.e., H2(A5), from N3-H of T6 at 13.60 ppm. Spectrum F shows NOE sites from N3-H of T7 at 13.89 ppm: a single NOE site is located at 7.34 ppm—hence the signals at (13.60, 7.34) ppm ought to belong to N3-H(T6) and H2(A5) of the A5-T6 pair near the internal 2-fold of the duplex (see the inset) which renders A5-T6 and T6-A5 chemically indistinguishable. In the inset, the NOE results are summarized: as indicated the primary NOEs originate from N3-H(T) → H2(A) both inside an A-T pair and in the 3′ → 5′ neighbor. Also, the pattern of primary NOEs from an NH of a base pair to both the neighbors is indicated.

The cross-peak for H2(A4)–H2(A3) at (7.07, 7.03) ppm is too close in chemical shift to be observed in this cross-section. The results of Figure 2 imply that H2(A)'s are less than 4.0 Å away from each other and form the core of the structural blocks containing A_4·T_4 and T_4·A_4 such that *N3H of ith A·T pair–H2 of (i + 1)th A·T pair* is closer in space than *N3H of ith A·T pair–H2 of (i–1)th A·T pair* as indicated earlier.

Assignment of the Proton System (H8/H6, H2/H5/CH3, H1′,H2′,H2″,H3′). At the outset, *H8's of A and G* were distinguished from *H6's of T and C* by selectively deuteriating H8 signals (Sarma et al., 1984) and comparing the NMR spectra of the base (H8/H6) regions of the normal and deuteriated samples.

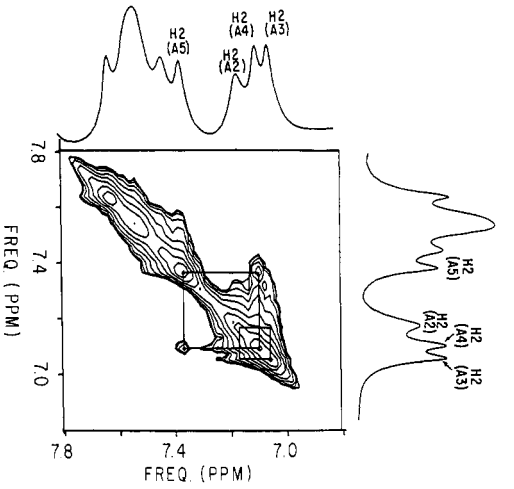

FIGURE 2: A NOESY cross section showing H2A–H2A cross-peaks for mixing time τ_m = 100 ms; the data matrix (t_2 = 1024 × t_1 = 512) was collected in the pure absorption mode (States et al., 1982) with a relaxation delay RD = 1.2 s—the HDO signal was presaturated. Figure 2 shows the *H2(A) vs H2(A)* NOESY cross section for τ_m = 100 ms. One cross-peak is seen at (7.34, 7.07) ppm which according to our assignment should correspond to H2(A5)–H2(A4).

A combination of NOESY data for τ_m = 100 and 50 ms and COSY data was used to arrive at the sequential assignment of the proton system [H8/H6, H2/H5/CH3, H1′,-H2′,H2″,H3′] belonging to 10 residues in $d(GA_4T_4C)_2$ at 12 °C. From an examination of primary NOEs as a function of τ_m's, we were able to conclude that the nucleotide geometry of each of the ten residues belongs to average C2′-endo,anti conformation as in a B-DNA because there was strong primary NOEs from the H8/H6 to the H2′,H2″ region but very small or almost zero NOEs to the H3′ region [for details of the methodology, see Sarma et al. (1985, 1986, 1987) and Gupta et al. (1985, 1987)]. When residues with C2′-endo,anti geometry are arranged in the gross morphology of a B-DNA duplex, one expects the NOE pattern H1′(i – 1)$\xrightarrow{3.0\text{–}3.8\ \text{Å}}$H8/H6($i$)$\xrightarrow{3.6\text{–}4.0\ \text{Å}}$H1′($i$) in the *H8/H6 vs H1′* cross section. In Figure 3A, the NOESY connectivity route for τ_m = 100 ms for H8/H6 → H1′ is shown. With A5 → T6 as a marker, the whole connectivity route is established, and this results in the sequential assignment of (H8/H6, H1′) of the 10 residues. Note that H5(C10) and H1′ (C10) occur at the same chemical shift value. The four CH3(T) signals are located in the region 1.7–1.1 ppm as sites of strong NOE from H6 (see Figure 4). In Figure 3B the *H8/H6 vs H1′* NOESY cross section is shown for τ_m = 50 ms. Note that at τ_m = 50 ms only internucleotide H1′ (i – 1) → H8/H6(i) NOEs prevail. It may be pointed out that H1's of T's are very close in chemical shift values (Table I) and not separately identifiable in Figure 3B. In Figure 3C the NOESY cross-section *H1′ vs H2′,H2″* is shown for τ_m = 50 ms. This enables us to sequentially assign (H1′,H2′,H2″) for the 10 residues. The chemical distinction between H2′ and H2″ of a residue is accomplished by inspecting the COSY cross section *H1′ vs H2′,H2″* (data not shown) where H1′–H2′ appear as stronger peaks than the corresponding H1′–H2″ peak (because for an average C2′-endo sugar $J_{1'2'} \sim 11$ Hz and $J_{1'2''} \sim 5$ Hz); H3's of the 10 residues are sequentially assigned from the *H3′ vs H2′,H2″* NOESY cross sections (data not shown). Therefore, combining all these data, we completed the sequential assignment

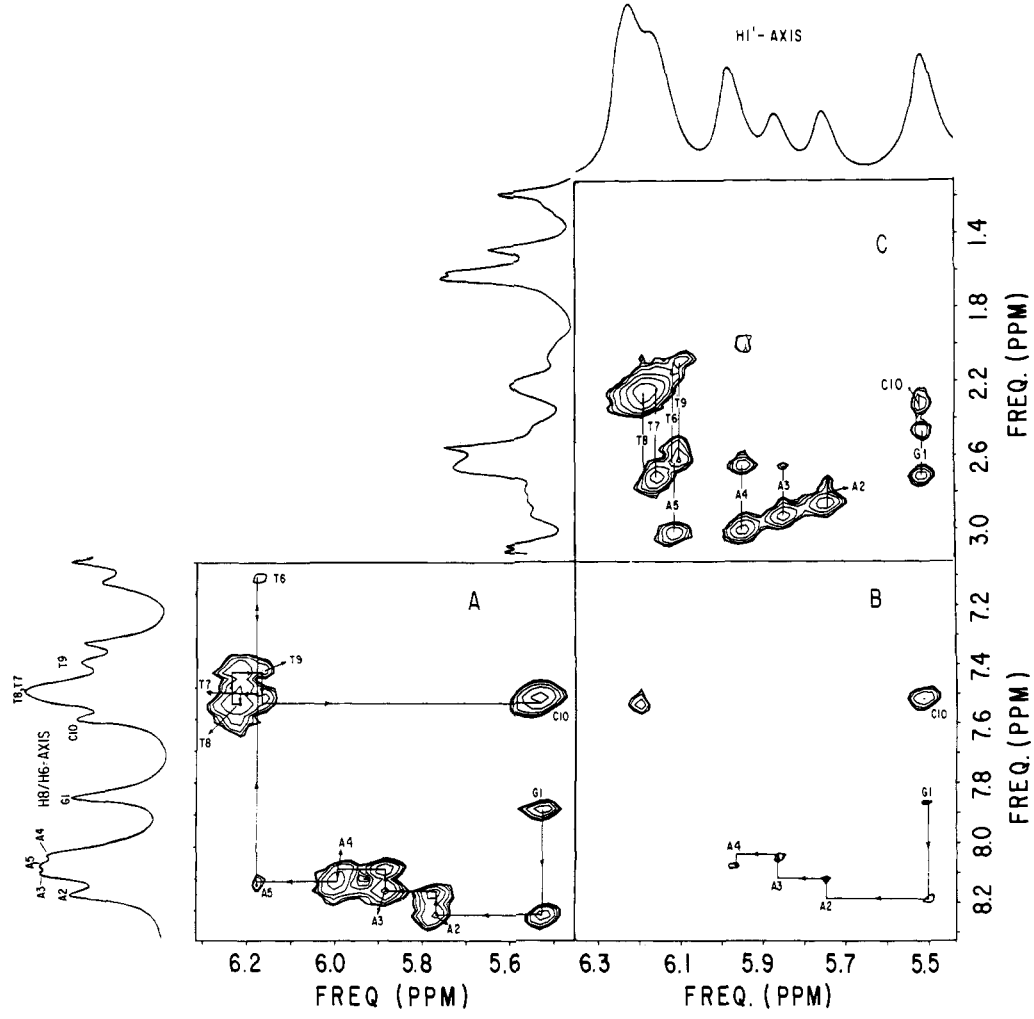

FIGURE 3: An assignment scheme of the proton system (H8/H6, H1',H2',H2'') of the 10 residues in the $d(GA_4T_4C)_2$ duplex in solution at 12 °C. NOESY experiments were conducted for $d(GA_4T_4C)_2$ (2 mM in duplex) in D_2O at 12 °C with other conditions the same as in Figure 2. In (A), the NOESY for the τ_m = 100 ms connectivity route involving H8/H6 → H1' is shown. With A5 → T6 connectivity as a marker, the whole connectivity route is established, which results in the assignment of H8/H6,H1' of the 10 residues. In (B), the same NOESY cross section is shown for τ_m = 50 ms; note the interresidue H1'(i − 1) → H8/H6 NOEs only prevail. It may be pointed out that H1's of Ts are very close in chemical shift values and hence not separately identifiable in (B). In (C), the NOESY (τ_m = 50 ms) cross section is shown for *H1' vs H2',H2''*. This enables us to identify the protons (H1',H2',H2'') for the 10 residues. This result is reconfirmed from the COSY spectrum for the *H1' vs H2',H2''* cross section where one observes H1'–H2' ($J_{1'2'}$ ~ 10 Hz) COSY peaks (data not shown).

Table I: Chemical Shift Values (ppm) of Various Protons in $d(GA_4T_4C)_2$ in Water at 12 °C with TSP as an Internal Standard

	H8/H6	H2/H5/CH3	H1'	H2',H2''	H3'	-NH
G1	7.88		5.53	2.50, 2.72	4.83	12.54
A2	8.21	7.17	5.77	2.73, 2.91	5.06	
A3	8.17	7.03	5.89	2.63, 2.90	5.06	
A4	8.10	7.07	5.98	2.63, 2.97	5.06	
A5	8.13	7.34	6.18	2.62, 3.00	5.06	
T6	7.16	1.20	6.18	2.06, 2.67	4.61	13.60
T7	7.49	1.52	6.22	2.13, 2.69	4.61	13.89
T8	7.54	1.63	6.26	2.27, 2.72	4.61	13.76
T9	7.41	1.68	6.16	2.09, 2.60	4.61	13.81
C10	7.55	5.53	5.53	2.25, 2.39	4.61	

of the proton system (H8/H6, H2/H5,CH3, H1',H2',H2'',-H3') of the 10 residues as listed in Table I. Assignments of H4',H5',H5'' are also made from the relevant NOESY cross section but not mentioned here.

In Figure 4A,B the NOESY cross sections *H8/H6 vs H2',H2''* are shown for τ_m = 100 and 50 ms. The connectivity route involving H2''(i − 1) → H8/H6 (i) → H2'(i) → H2''(i) reflects the true nature of an oligomer duplex in the gross morphology of B-DNA. Also shown in Figure 4A,B are the connectivity routes involving H6T(i − 1) → CH3T(i) → H6T(i) (marked by broken lines).

Primary Observations. The NMR data presented, so far, indicate the following structural features about the d-$(GA_4T_4C)_2$ duplex:

(i) The two structural blocks d(Gl-A2-A3-A4-A5)·d(T6-T7-T8-T9-C10) and d(T6-T7-T8-T9-C10)·d(G1-A2-A3-A4-A5) are conformationally identical, and there is an internal twofold because there is no resonance doubling for the same protons on the two strands. Particularly striking is the NOE at the site of the structural twofold from N3H of T6 to H2 of A5 in the opposite strand as well as to H2 of A5, its 5' neighbor (Figure 1F).

(ii) The NOESY data for τ_m = 100 ms reveal the proximity of H2(A)'s along the chain (Figure 2). The fact that H2-(A)–H2(A) cross-peaks are also observed at τ_m = 50 ms suggests that the distance between the H2(A)'s in two neighboring residues may be below 3.5 Å (the cutoff distance for the NOESY data at τ_m = 50 ms).

(iii) One-dimensional NOE results in H_2O (Figure 1) show that the *N3H of ith A·T pair–H2 of* (i + 1)*th A·T pair* is closer in space than the *N3H of ith A·T pair–H2 of* (i − 1)*th A·T pair*: indicating a large propeller twist (≥15°) in the A·T pairs.

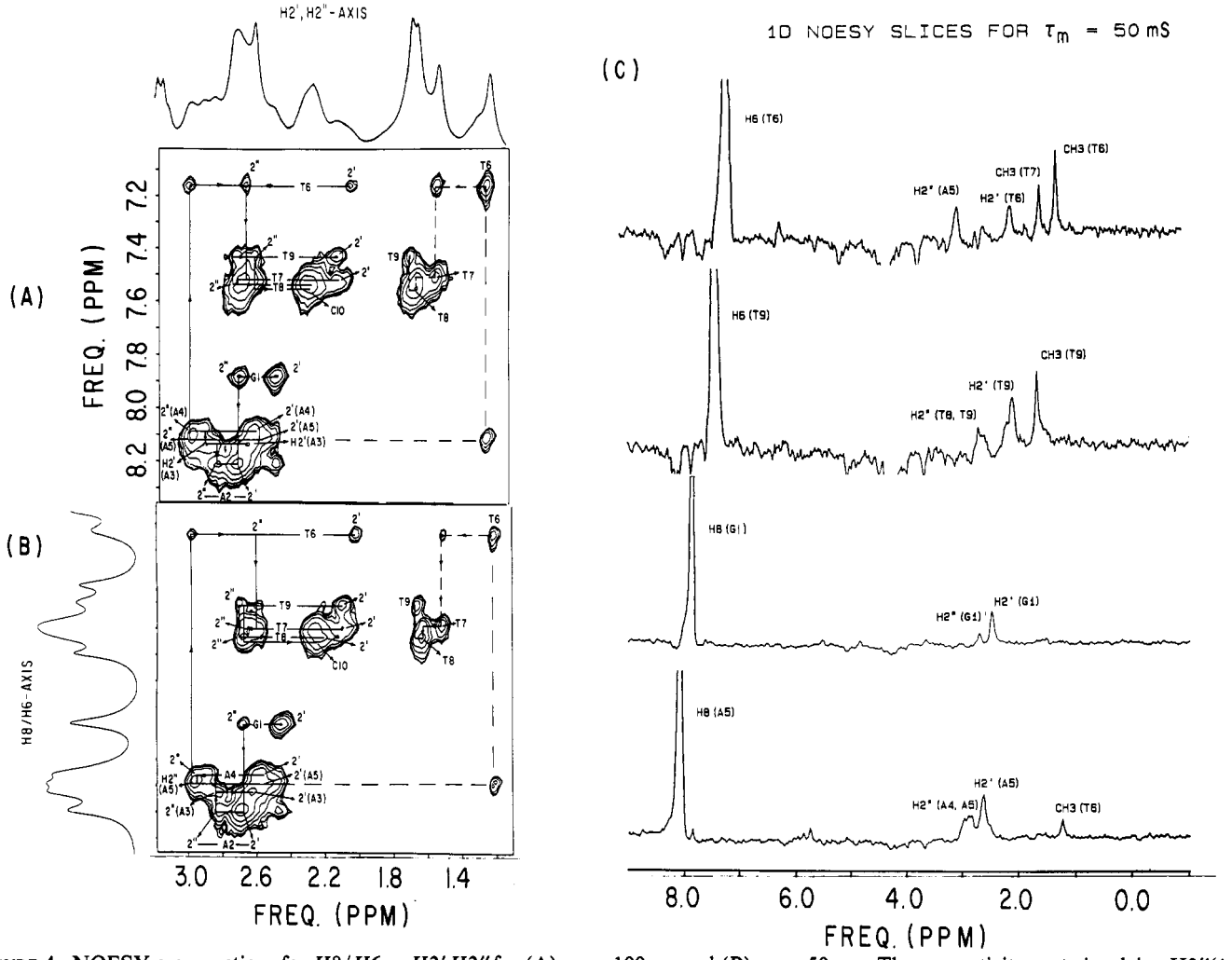

FIGURE 4: NOESY cross sections for *H8/H6 vs H2',H2''* for (A) τ_m = 100 ms and (B) τ_m = 50 ms. The connectivity route involving H2''(i − 1) → H8/H6(i) → H2'(i) etc. is exactly as expected from a B-DNA duplex with residues in average C2'-endo,anti geometry. The cross-connectivity route involving the CH3(T) protons is also shown (marked by broken line). Inspection of the 1D NOESY slices through H8/H6 (C) indicated that intranucleotide H8/H6(i) → H2'(i) NOEs were stronger than the corresponding internucleotide H8/H6(i) → H2''(i − 1) NOEs; one exception was the NOEs for H6(T6) → H2'(T6) and H6(T6) → H2''(A5), which were of equal intensity as evident from the 1D slices of the NOESY data at τ_m = 50 ms which essentially manifested primary NOEs. This suggested that there was a subtle discontinuity at A5 → T6. As shown in (C), the NOE from H8(A5) to H2'(A5) is stronger (by 2-fold) than the combined NOEs from H8(A5) to H2''(A5) and H2''(A4) [because H2''(A4) and H2''(A5) have overlapping chemical shifts, see Table I]. Similarly from (C) we observe that the NOE from H6(T9) to H2'(T9) is about 2-fold stronger than the combined NOEs at H2''(T9) and H2''(T8) (close in chemical shift, see Table I). In panel C also is inlcuded the 1D slice showing the NOE from H8(G1) to H2'(G1) and H2''(G1)—about 6 times weaker NOE at H2''(G1) indicates that at τ_m = 50 ms higher order NOEs are very small.

(iv) Inspection of primary NOE at τ_m = 50 ms from CH3(T)'s showed that the CH3(T_i)–H6(T_i) NOE is nearly as strong as that of CH3(T_i)–H6(T_{i-1}) (data not shown). This indicates that in the two structural blocks the corresponding distances are close (CH3(T)–H6(T) ~ 3.0 Å—a fixed distance).

(v) In Figure 4C 1D slices are shown for the NOESY data for τ_m = 50 ms. As representative examples, four slices through H8(G1), H8(A5), H6(T6), and H6(T9) are shown. Notice that, NOEs from H8(A5) to H2'(A5) are larger (by about 2-fold) than the NOE from H8(A5) to H2''(A5)/H2''(A4) (H2'' of A4,A5 overlap in chemical shifts, see Table I); similarly, NOEs from H8(T9) to H2'(T9) are about 2-fold larger than the NOEs from H6(T9) to H2''(T9)/H2''(T8) (H2''s of T8,T9 are close in chemical shfts, see Table I). The 1D slice through H8(G1) shows a strong NOE at H2'(G1) and a weaker (by 5-fold) NOE at H2''(G1)—this indicates that at τ_m = 50 ms the higher order NOEs are only marginal and NOE can reflect a true measure of direct interproton distances.

(vi) Comparison of the spectra in Figure3A,B show that internucleotide H1'(i − 1)–H8/H6(i) is shorter in distance than the intranucleotide H1'(i)–H8/H6(i) distance (especially for the A's).

Untenability of a Conventional Fiber B-DNA Model for $d(GA_4T_4C)_2$. Even though the geometry of each nucleotide residue grossly resembles that of a classical B-DNA, i.e., C2'-endo,anti, the following observations argue against a classical straight B-DNA structure for $d(GA_4T_4C)_2$:

(a) In the fiber B-DNA model (Arnott et al., 1980) the intranucleotide NOE involving H2'(i)–H8/H6(i) (distance ~2.2 Å) is expected to be weaker than the internucleotide NOE involving H2''(i − 1)–H8/H6(i) (distance ~2.0 Å). Our NOESY data show that for nine residues in the $d(GA_4T_4C)_2$ the intranucleotide NOE involving H2'(i)–H8/H6(i) is stronger than the internucleotide NOE involving H2''(i − 1)–H8/H6(i); the only exception is the T6 residue in which NOEs involving H2''(T6)–H6(T6) and H2''(A5)–H6(T6) are of equal intensity.

(b) In the fiber B-DNA model of Arnott et al. (1980), the H2(A_i)–H2(A_{i+1}) distance is ~3.8 Å. Our NOESY data at τ_m = 100 and 50 ms show NOEs involving H2(A_i)–H2(A_{i+1});

the presence of such NOEs even at a lower τ_m = 50 ms suggests that H2(A_i)–H2(A_{i+1}) distances in d(GA_4T_4C)$_2$ may be ~3.5 Å.

Structural Alternations in the Fiber B-DNA Model To Fit the NOE Data of d(GA_4T_4C)$_2$: Its Shortcomings. We have attempted to construct and refine a straight B-DNA duplex for d(GA_4T_4C)$_2$ in order to explain the discrepancies cited above. In Figure 5A, two stereoviews of this model are shown. However, this model could not explain the following two observations:

(a) The H2(A_i)–H2(A_{i+1}) distance in this model was 3.9 Å.

(b) The NOEs predicted for this model for the T6 residue were in disagreement with the observed values; i.e., for this model NOEs for H2′(T6)–H6(T6) at τ_m = 100 and 50 ms are expected to be 2-fold stronger than NOEs for H2″(A5)–H6(T6) while the corresponding experimental NOEs are of equal intensity.

A Junction B-DNA Model for d(GA_4T_4C)$_2$. The concept of a junction model as a probable cause of bending was first introduced by Crothers and co-workers (Levene & Crothers, 1983). They aruged that a junction was formed when a heteronomous DNA structure for a d$(A)_n$·d$(T)_n$ tract was joined with a classical B-DNA structure for other neighboring sequences. However, our NOE data on d(GA_4T_4C)$_2$ duplex unequivocally ruled out the possibility of the heteronomous structure of Arnott et al. (1983) [proposed to explain the fiber data on poly[d(A)]·poly[d(T)] for the two structural blocks A_4·T_4 and T_4·A_4. In fact, we clearly show that these structural blocks are conformationally equivalent and both A and T residues belong to C2′-endo,anti geometry. The NOE data provided no evidence of the presence of C3′-endo pucker for either A or T residue. This observation was consistent with our earlier work on poly[d(A)]·poly[d(T)] in solution (Sarma et al., 1985) where we clearly provided the direct experimental data suggesting that in this polymer both A and T residues adopt C2′-endo,anti geometry. Later on, Alexeev et al. (1987) showed that the so-called "heteronomous DNA model" was not even valid for poly[d(A)]·poly[d(T)] in fiber. Also, the conclusions of Sarma et al. (1985) on poly[d(A)]·poly[d(T)] structure in solution were reconfirmed by Behling and Kearns (1986).

A very important observation is the unique NOE pattern from H6(T6) (Figure 4C). Among the 10 residues only H6(T6) shows equally intense NOEs at H2′(T6) and H2″-(A5). In all other residues, the NOEs for H2′(i)–H8/H6(i) are stronger than the NOEs for H2″(i − 1)–H8/H6(i). This suggests that the structural frames of two conformally equivalent blocks [i.e., d(G1-A2-A3-A4-A5)·d(T6-T7-T8-T9-C10) and d(T6-T7-T8-T9-C10)·d(G1-A2-A3-A4-A5)] do not coincide and there is a finite discontinuity at the A5 → T6 junction. The task at hand is to derive a structure in which two conformationally equivalent structural blocks are joined in such a way that fit the observed NOE pattern from H6(T6) (Figure 4C), while the H2(A_i)–H2(A_{i+1}) distances in each structural blocks are maintained at ~3.5 Å. In addition, such a structure should explain all observed NOEs, taking into account the contribution to NOE intensities from primary, secondary, and all higher orders of magnetization transfer.

We are aware of the fact that the T1 values of H2 of A's may be longer than 1.2 s, the value of RD that we used in our NOESY experiments. Thus, before each mixing phase of the pulse sequence, H2's of A's may not have completely recovered to 100% population. But this does not undermine our conclusion regarding the proximity of H2A–H2A cross-peaks. It may be pointed out that the H2A–H2A cross-peaks are not treated at the same quantitative level as the other proton pairs in Table II. By monitoring the presence or absence of H2A–H2A cross-peaks, we make a judgement whether the corresponding H2A–H2A distances are above or below the cutoff distance for the corresponding τ_m.

The best way of deriving such a structure is to start with a qualitative model and simulate the NOESY intensities in the model (see NOESY Data Simulation). The structural model is continuously refined until a satisfactory agreement is reached between the observed and calculated NOE intensities at all the employed mixing times.

We have been able to derive such a structural model for d(GA_4T_4C)$_2$. This model, which we called "junction B-DNA model" as discussed earlier, is shown in Figure 5B as a stereo pair. In the junction B-DNA model, without violating any stereochemical constraints, it was necessary to arrange the chains d(GA_4) and d(T_4C) to be not equidistant from the local frame of reference so that the H2(A_i)–H2(A_{i+1}) distance is ~3.5 Å, consistent with AH2 NOE cross-peaks.

Computer-simulated NOESY data for the junction B-DNA model are shown in Table II. Similar data for the straight B-DNA model are not shown in Table II but are available upon request. There is satisfactory agreement between observed NOE intensities and those calculated for the junction B-DNA model, considering the fact that we have used only one τ_c. In Table II, the calculated (and observed) NOESY intensities are tabulated for an overall correlation time τ_c = 4 ns. An estimate of τ_c was obtained by monitoring the NOE as a function of τ_m for a proton pair with fixed distance (viz., H6C–H5C, H6T–CH3T). In refining of the junction B-DNA model and seeking the agreement between the observed and simulated NOESY intensities for τ_m = 100 and 50 ms, all NOEs involving H8/H6, H2/H5/CH3, and H1′,H2′,H2″,H3′ were considered although Table II shows only a few representative ones for τ_m = 50 ms. For a set of overlapping signals, computed NOESY intensities of individual signals were added before comparison with the observed value. The total number of about 20 NOE intensities involving various protons was available to define the geometry of a residue, and for 10 residues in d(GA_4T_4C)$_2$ we had about 10 × 20 = 200 intensity values for *each mixing time*. In the simulation procedure all the intensity data were used for each mixing time to arrive at the final model.

In order to illustrate the applicability of our simulation procedure, we list in Table II the calculated and observed NOESY intensity values for a set of base protons H8/H6 for which the 1D NOESY slices for τ_m = 50 ms are enclosed in Figure 4C. Considering the fact that the junction B-DNA model was simulated for an isotropic overall τ_c (as a first approximation), the calculated NOESY intensities for the protons H8/H6, H2/H5/CH3, H1′,H2′,H2″,H3′ of all the 10 residues show satisfactory agreement with the observed NOESY intensity data for τ_m = 100 and 50 ms. A complete comparison of the calculated NOESY intensities for τ_m = 100 and 50 ms for various protons and the corresponding observed 1D NOESY slices is beyond the scope of this short paper and will be reported elsewhere. The inclusion of selected 1D NOESY slices for τ_m = 50 ms and the corresponding calculated NOESY intensities in Table II bring forth the physical basis of our junction B-DNA model. A5 and T9 are the two residues present in the two structural blocks in the decamer, i.e., d(G1-A2-A3-A4-A5)·d(T6-T7-T8-T9-C10) and d(T6-T7-T8-T9-C10)·d(G1-A2-A3-A4-A5). Note that for both H8(A5) and H6(T9) the NOEs for τ_m = 50 ms, H8(A5)–

Table II: Representative Observed Percent NOEs at τ_m = 50 ms for $d(GA_4T_4C)_2$ and Those Calculated for the Finally Refined Junction Model (Figure 5B) with a τ_c = 4 ns and Curved Model (Figure 5C) with a τ_c = 5 ns[a]

% NOE from	to	to	to	to	to	to
H8(G1)	H2′(G1)	H2″(G1)	H1′(G1)			
I	7	2	–			
II	8	1	–			
III	5	–	–			
H8(A2)	H2′(A2)/H2″G1	H2′(G1)	H2″(A2)		H1′(A2)	H1′(G1)
I	14	3	4		–	1
II	14	1	2		–	1
III	10	1	1		–	1
H8(A4)	H2′(A4)	H2″(A4)/H2″(A3)	H1′(A4)		H1′(A3)	
I	10	8	–		1	
II	9	7	–		1	
III	7	6	–		–	
H8(A5)	H2′(A5)	H2″(A5)/H2″(A4)	H1′(A4)		CH3(T6)	
I	9	6	–		3	
II	8	5	1		2	
III	7	4	–		–	
H6(T6)	H2′(T6)	H1′(T6/A5)	H2″(T6)/H2′(A5)	H2″(A5)	CH3(T6)	CH3(T7)
I	8	2	2	8	18	8
II	7	1	2	8	12	6
III	9	1	3	7	12	4
H6(T7)	H2′(T7)	H2″(T7)/H2″(T6)	H1′(T7)/H1′(T6)	CH_3(T7)	CH_3(T8)	
I	6	4	–	11	8	
II	6	5	–	12	5	
III	9	10	–	12	2	
H6(T8)/H6(C10)	H2′(T8)/H2′(C10)	H2″(T8)/H2″(T7)	H1′(T8)/H1′(T7)	CH3(T8)/CH3(T9)	H1′(T9)	H1′(C)/H5(C10)
I	14	8	3	16	–	4
II	13	5	1	12	–	5
III	15	7	–	12	–	5
H6(T9)	H2′(T9)	H2″(T9)/H2″(T8)	H1′(T9)/H1′(T8)	CH3(T9)	H5(C10)	
I	8	5	–	15	–	
II	6	5	–	12	–	
III	9	7	–	12	–	

[a] Complete set of data is available on request. Similar data for the straight B-DNA model (Figure 5A) are also available upon request. % NOE = [(peak height at the site of NOE)/(height of peak through which the slice was taken)] × 100. Two overlapping signals are put on top of the same intensity column in the table; viz., overlapping H2″(A4) and H2″(A3) are listed as H2″(A4)/H2″(A3) on top of the same intensity column. Intensity heights below 1% are marked (–). Row I gives the observed values at τ_m = 50 ms. Row II lists the values calculated for the final junction B-DNA model, and row III gives the calculated values for the final curved B-DNA model.

H2′(A5) and H6(T9)–H2′(T9), are stronger by about twofold than the NOEs H8(A5)–H2″(A4) and H6(T9)–H2″(T8)—clearly seen from Figure 4C and Table II. However, for the residue T6, the nucleotide connecting the two structural blocks, the NOE H6(T6)–H2′(T6) is as strong as H6(T6)–H2″(A5) for τ_m = 50 ms—see Figure 4C and Table II. Notice that the calculated NOESY intensities for τ_m = 50 ms for the junction B-DNA model show agreement with the corresponding observed intensities for the protons H8(A5), H6(T9), and H6(T6) (see Table II and Figure 4C). Also included in Figure 4C is the NOESY slice for H8(G1) for τ_m = 50 ms to show that only sites of NOEs are at H2′(G1) and H2″(G1): the NOE at H2′(G1) [H8(G1)–H2′(G1) = 2.3 Å] being about fivefold stronger than that at H2″(G1) [H8(G1)–H2″(G1) = 3.9 Å]. This indicates that at τ_m = 50 ms, the spin diffusion H8(G1)$\xrightarrow{2.3\text{ Å}}$H2′(G1)$\xrightarrow{1.8\text{ Å}}$H2″(G1) is reduced to a bare minimum and at τ_m = 50 ms NOEs from various protons in effect reflect a primary NOE pattern. See Table II for comparison of calculated and observed values for H8(G1). The calculated and observed NOEs from H8(A2), H8(A4), H6(T7), and H6(T8/C10) are also included in Table II (although the corresponding slices are not shown in Figure 4C): note that for these protons, too, the junction B-DNA model gives a satisfactory agreement with the observed data. It may be noted that for the straight B-DNA model the caluclated NOESY intensities (for τ_c = 4 ns) for H6(T6)–H2′(T6) and H6(T6)–H2″(A5) cross-peaks are 18 and 9 for τ_m = 100 ms and they are 11 and 5 for τ_m = 50 ms. For the junction B-DNA model, intensities for H6(T6)–H2′(T6) and H6(T6)–H2″(A5) are 12 and 12 for τ_m = 100 ms (corresponding observed values being 11 and 11), and the calculated intensities of the same cross-peaks for τ_m = 50 ms are 7 and 8 (corresponding observed values being 8 and 8). Thus, the straight B-DNA model is in clear disagreement with respect to the observed NOESY intensities for H6(T6)–H2′(T6) and H6(T6)–H2″(A5).

The conformation parameters for the straight B-DNA model (Figure 5A) are [following the notation of Saenger (1984)] α = 314°, β = 150°, γ = 50°, δ = 137°, ϵ = 210°, ξ = 225°, χ = 255°, base tilt θ_x = −2°, propeller twist between the bases in a base-pair θ_y = 8°, and displacement of the base pair center from the helix center D = 0.4 Å [notations θ_x, θ_y, and D have the same meaning as in Arnott et al. (1969)]. Note that, in the straight B-DNA model all the 10 residues in the decamer duplex do have the same conformational parameters. As stated earlier, simulation of this straight B-DNA model mimics all the observed NOESY intensities except at the A5 → T6 junction and for H2(A_i)–H3(A_{i+1}) cross-peaks.

In the junction B-DNA model (Figure 5B), the purines (A and G) are conformationally nonequivalent from the pyrimidines (T and C). For the two blocks d(G1-A2-A3-A4-A5)·d(T6-T7-T8-T9-C10) and d(T6-T7-T8-T9-C10)·d(G1-A2-A3-A4-A5), *for A and G* α = 320°, β = 135°, γ = 40°, δ = 138°, ϵ = 220°, ξ = 200°, and χ = 265°, and *for T and C* α = 330°, β = 165°, γ = 40°, δ = 119°, ϵ = 180°, and χ = 250°. Note that the torsion angles for both chains fall within the observed range of values for the B-DNA dodecamer crystal (Fratini et al., 1982). In this structure both purines (A, G) and pyrimidines (T, C) have very small tilt.

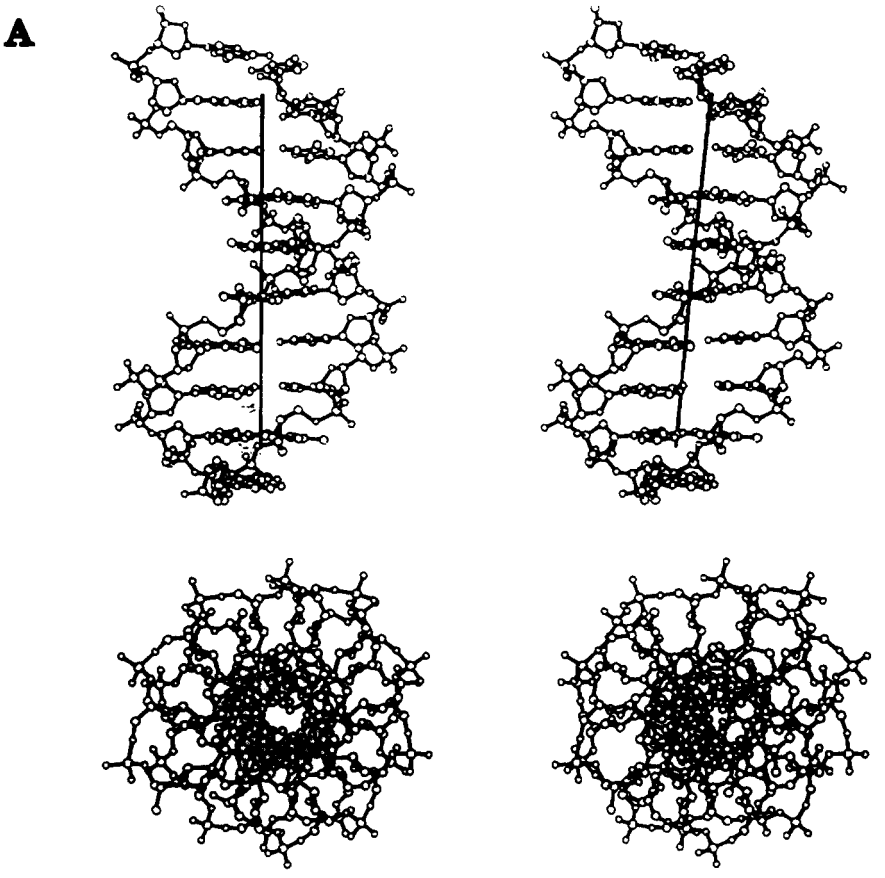
A

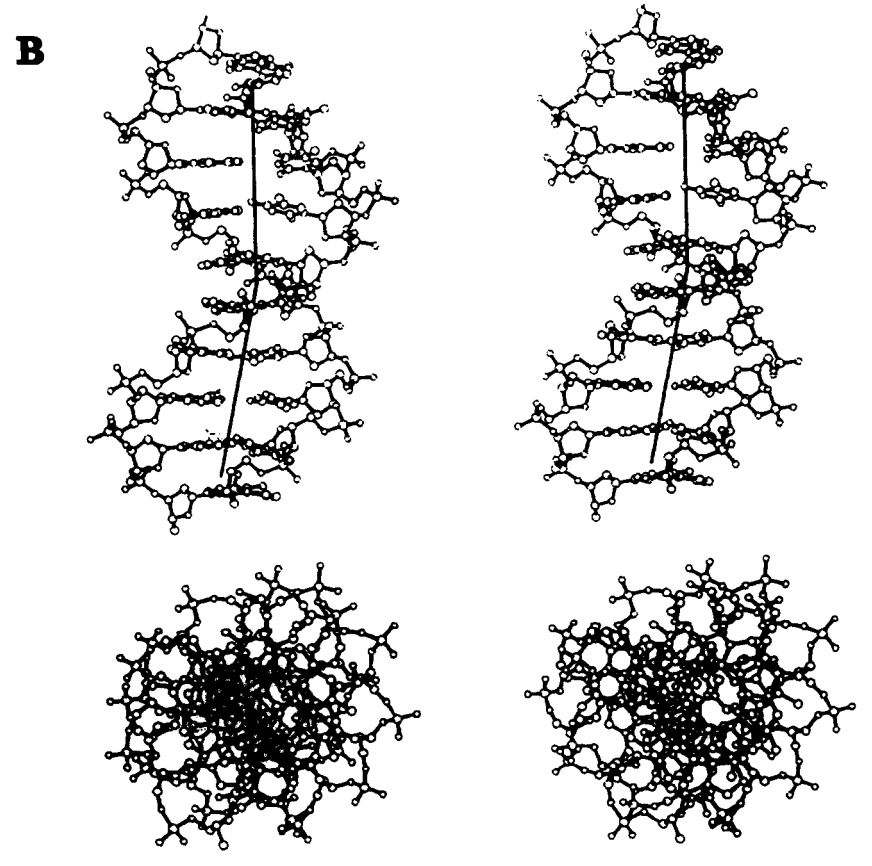
B

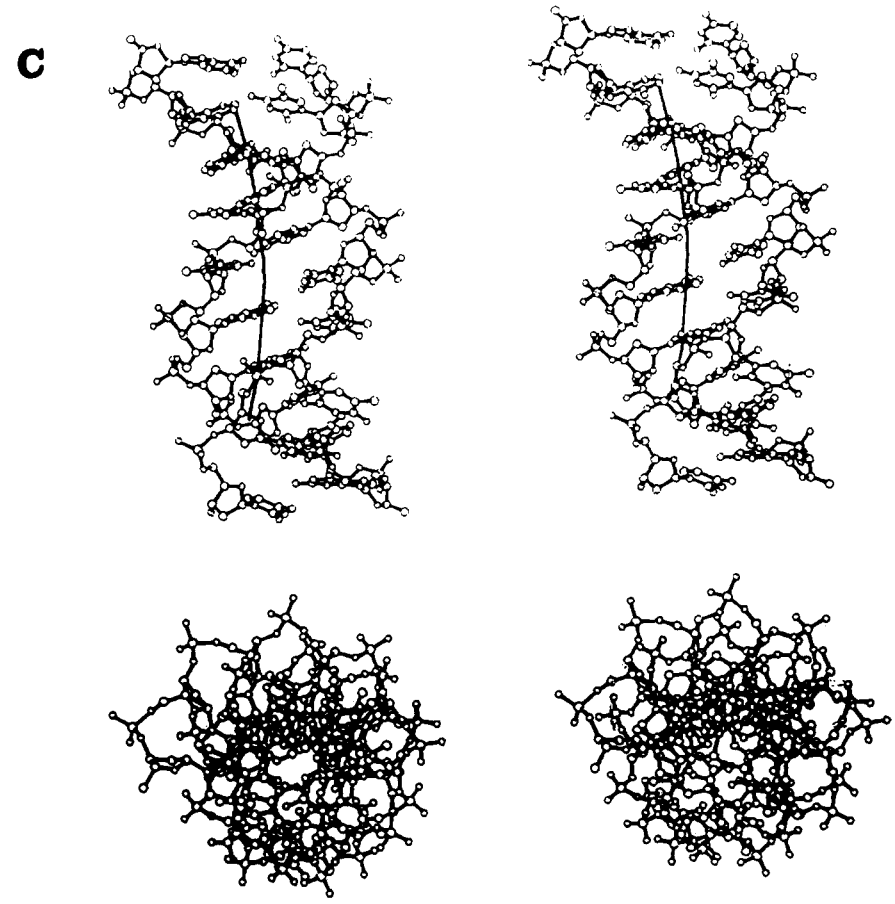

FIGURE 5: (A) Two views of stereopairs of the straight B-DNA model: (top) ball and stick along the long axis and (bottom) ball and stick down the long axis. (B) Two steropairs of the junction B-DNA model for $d(GA_4T_4C)_2$ projected along two mutually perpendicular axes. Note that in this model the two structural frames of reference at the A5 → T6 junction do not coincide in space as shown by two local frames creating a discontinuity at the A5 → T6 junction. For conformational details of these models, see the text. Note that in the downview of the two models it became clear that in the junction B-DNA model two strands $d(GA_4)$ and $d(T_4C)$ are situated at different distances from the center of the molecule while in the straight B-DNA model ($d(GA_4)$ and $d(T_4C)$ chains are equidistant from the center of the molecule. (C) Two views of the smoothly curved B-DNA model for $d(GA_4T_4C)_2$. Note that in this model the long axis of the duplex traces a curved path as shown in the diagram.

However, the A-T pairs have a large propeller twist of 15°. Small adjustments were made in χ's for G and C to reduce the θ_y to 7° in a G-C pair so that three perfect H bonds are formed. Note that when the two structural blocks, i.e., d(G1-A2-A3-A4-A5)·d(T6-T7-T8-T9-C10) and d(T6-T7-T8-T9-C10)·d(G1-A2-A3-A4-A5), are joined by utilizing the flexibility at the P–O bonds [i.e., angles (ξ, α)] subject to favorable dyad-related stacking at

two local frames do not coincide. This might result in originating a potential nucleation center for bending as shown by two local frames forming a discontinuity (Figure 5B). The conformational features at the A5 → T6 junction on both the strands are

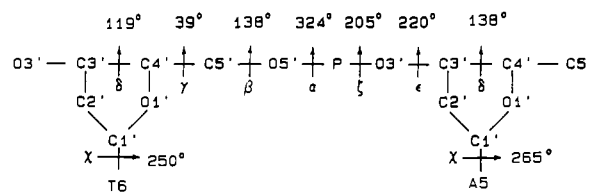

In our junction model A·T pairs in both the structural blocks are perpendicular to the local helix axis. The phosphate groups attached to T's are 8.8 Å away from the local helix center (i.e., R_p for T's ~ 8.8 Å), while the phosphate groups attached to the A's are 9.7 Å away from the local helix center (i.e., R_p for A's ~ 9.7 Å). The closest distance of approach between two phosphate groups on opposite strands in the minor groove is 11 Å (i.e., S_p ~ 11 Å). Our junction model creates an overall bending of 10° with a center of curvature 50 Å away from the center of the duplex.

We also completed the NOESY data simulation of a curved B-DNA model for $d(GA_4T_4C)_2$. The curved B-DNA model was generated with the method of Levitt (1978)—the model approximates the AA-wedge model of Trifonov (1986). The details of the curved B-DNA model and a brief discussion of motional dynamics on calculated NOESY intensity are provided as supplementary material. A complete set of molecular diagrams are also included in the supplementary material (see paragraph at end of paper regarding supplementary material).

Discussion

Our observation that the presence of a junction creates bent DNAs is in keeping with the recent crystallographic observation of Nelson et al. (1987) on the dodecamer duplex d(CGCA$_6$GCG)·d(CGCT$_6$GCG). In this molecule, there is a large propeller twist of average 20° in the six A·T pairs, but the six A·T pairs in the structural block A_6·T_6 are perpendicular to the local helix axis. At each junction of the structural block A_6·T_6, there is a finite discontinuity in the molecule which the authors suggest as the most probable cause of bending for DNA sequences with A_n·T_n tracts regularly in-

terrupted by other sequences as in the kinetoplast DNA. In the dodecamer (Nelson et al., 1987) the junction occurs at C → A, A → G, C → T, T → G; in our junction B-DNA the junction is centrally located at A5 → T6. However, the crystal analysis of Nelson et al. (1987) on the dodecamer and our solution structural analysis point to a general conclusion; i.e., junction formation may be the most probable cause of bending. Our observation that the A → T sequence joining two $A_n \cdot T_n$ blocks is a potential site of bending is also consistent with the gel electrophoretic analysis of Hagerman (1986). Hagerman observed that in the polymer $d(GA_4T_4C)_{n\geq 10}$ the replacement of terminal G by C (or C by G) still produced a bent DNA duplex. Hagerman (1986) also observed that the polymer $d(GT_4A_4C)_{n\geq 10}$ behaved like a straight DNA duplex. Hence, one can conclude from Hagerman's data that the A → T sequence joining two $A_n \cdot T_n$ blocks may be an important cause of bending, and our solution NMR data on $d(GA_4T_4C)_2$ duplex also corroborate the same fact. Very recently, Coll et al. (1987) determined the crystal structure of $d(CGCA_3T_3GCG)_2$ at 2.2-Å resolution. The structure reveals a large propeller twist (of about 20°) in the A·T pairs and junctions located at C → A and T → G sequences. The structure solution at 2.2-Å resolution indicates that A_3T_3 stretch is essentially straight and there is no junction formation at the central A → T sequence which is contrary to what we observe for $d(GA_4T_4C)_2$ from our solution NMR data.

ACKNOWLEDGMENTS

We gratefully acknowledge the technical assistance of Virginia E. Dollar.

SUPPLEMENTARY MATERIAL AVAILABLE

Details of the curved B-DNA model and a brief discussion of motional dynamics on calculated NOESY intensity and three figures depicting a complete set of molecular diagrams (7 pages). Ordering information is given on any current masthead page.

REFERENCES

Alexeev, D. G., Lipanov, A. A., & Skuratovskii, I. Ya. (1987) *J. Biomol. Struct. Dyn. 4*, 989–1012.

Arnott, S., Dover, S. D., & Wonacott, A. J. (1969) *Acta Crystallogr., Sect. B: Struct. Crystallogr. Cryst. Chem. B25*, 2192–2199.

Arnott, S., Chandrasekaran, R., Birdsall, D. L., Leslie, A. G. W., & Ratliff, R. L. (1980) *Nature (London) 283*, 743–745.

Arnott, S., Chandrasekaran, R., Hall, I. H., & Puigjaner, L. C. (1983) *Nucleic Acids Res. 11*, 4141–4152.

Behling, R., & Kearns, D. R. (1986) *Biochemistry 25*, 8473.

Broido, M. S., James, T. L., Jon, G., & Keepers, J. W. (1985) *Eur. J. Biochem. 150*, 117–128.

Coll, M., Frederick, C. A., Wang, A. H.-J., & Rich, A. (1987) *Proc. Natl. Acad. Sci. U.S.A. 84*, 8385–8389.

Fratini, A. V., Kopka, M. L., Drew, H. R., & Dickerson, R. E. (1982) *J. Biol. Chem. 254*, 14686–14707.

Frederick, C. A., Grable, J., Melia, M., Samudzi, C., Jen-Jacobson, L., Wang, B.-C., Green, P., Boyer, J. W., & Rosenberg, J. M. (1984) *Nature (London) 309*, 309–314.

Gupta, G., Sarma, M. H., & Sarma, R. H. (1985) *J. Mol. Biol. 186*, 463–469.

Gupta, G., Sarma, M. H., Sarma, R. H., Bald, R., Engelke, U., Oei, S. L., Gessner, R., & Erdmann, V. A. (1987) *Biochemistry 26*, 7715–7723.

Hagerman, P. J. (1984) *Proc. Natl. Acad. Sci. U.S.A. 81*, 4632–4636.

Hagerman, P. J. (1986) *Nature (London) 321*, 1149–1150.

Keeper, J. W., & James, T. L. (1984) *J. Magn. Reson. 57*, 404–429.

Kifchin, P., Klein, V. A., Ryan, K. A., Gann, K. L., Rauch, C., Kang, D. S., Wells, R. D., & Englund, P. T. (1983) *J. Biol. Chem. 261*, 11301–11310.

Levene, S. D., & Crothers, D. M. (1983) *J. Biomol. Struct. Dyn. 1*, 429–435.

Levitt, M. (1978) *Proc. Natl. Acad. Sci. U.S.A. 75*, 640–644.

Marini, J. C., Levene, S. D., Crothers, D. M., & Englund, P. T. (1982) *Proc. Natl. Acad. Sci. U.S.A. 79*, 7664–7668.

Matteuci, M. D., & Caruthers, M. H. (1981) *J. Am. Chem. Soc. 103*, 3185–3191.

Nelson, H. C. M., Finch, J. T., Luisi, B. F., & Klug, A. (1987) *Nature (London) 330*, 221–226.

Olson, W. K., Srinivarsan, A. R., Hao, M., & Nauss, J. L. (1988) *Structure & Expression* (Olson, W. K., Sarma, M. H., Sarma, R. H., & Sundaralingam, M., Eds.) Vol. 3, pp 225–242, Adenine, Guilderland, NY.

Roy, S., Borah, G., Zon, G., & Cohen, J. S. (1987) *Biopolymers 26*, 525–633.

Saenger, W. (1984) in *Principles of Nucleic Acid Structures*, Springer-Verlag, New York.

Sarma, M. H., Gupta, G., & Sarma, R. H. (1984) *J. Biomol. Struct. Dyn. 1*, 1423–1455.

Sarma, M. H., Gupta, G., & Sarma, R. H. (1985) *J. Biomol. Struct. Dyn. 2*, 1057–1084.

Sarma, M. H., Dhingra, M. M., Gupta, G., & Sarma, R. H. (1986) *Biochemistry 25*, 3659–3665.

Sarma, M. H., Gupta, G., Sarma, R. H., Bald, R., Engelke, U., Oei, S. L., Gessner, R., & Erdmann, V. A. (1987) *Biochemistry 26*, 7707–7714.

States, D. J., Haberkorn, R. H., & Ruben, D. J. (1982) *J. Magn. Reson. 48*, 286–292.

Trifonov, E. N. (1986) *CRC Crit. Rev. Biochem. 19*, 89–106.

Ulanovsky, L. E., & Trifonov, E. N. (1987) *Nature (London) 326*, 720–722.